Tunable giant exchange bias in the single-phase rare-earth–transition-metal intermetallics $YMn_{12-x}Fe_x$ with highly homogenous intersublattice exchange coupling

Yuanhua Xia,[1,2] Rui Wu,[1,2] Yinfeng Zhang,[1,2] Shunquan Liu,[1,2,*] Honglin Du,[1,2] Jingzhi Han,[1,2] Changsheng Wang,[1,2] Xiping Chen,[3] Lei Xie,[3] Yingchang Yang,[1] and Jinbo Yang[1,2,4,†]

[1]*State Key Laboratory for Mesoscopic Physics, School of Physics, Peking University, Beijing 100871, People's Republic of China*

[2]*Beijing Key Laboratory for Magnetoelectric Materials and Devices, Beijing 100871, People's Republic of China*

[3]*Institutes of Nuclear Physics and Chemistry, China Academy of Engineering Physics, Mianyang 621999, China*

[4]*Collaborative Innovation Center of Quantum Matter, Beijing 100871, People's Republic of China*

(Received 12 April 2017; revised manuscript received 7 July 2017; published 30 August 2017)

A tunable giant exchange bias effect is discovered in a family of bulk intermetallic compounds $YMn_{12-x}Fe_x$. Experimental data demonstrate that the exchange bias effect originates from global interactions among ferromagnetic and antiferromagnetic sublattices but not the interfacial exchange coupling or inhomogeneous magnetic clusters. A giant exchange bias with a loop shift of up to 6.1 kOe has been observed in $YMn_{4.4}Fe_{7.6}$ compound. In a narrow temperature range, the exchange bias field shows a sudden switching-off whereas the coercivity shows a sudden switching-on with increasing temperature. This unique feature indicates that the intersublattice exchange coupling is highly homogenous. Our theoretical calculations reveal this switching feature, which agrees very well with the experiments and provides insights into the physical underpinnings of the observed exchange bias and coercivity.

DOI: 10.1103/PhysRevB.96.064440

I. INTRODUCTION

The exchange bias (EB), which usually refers to a shift of the hysteresis loop along the field axis in the exchange coupled ferromagnetic (FM)/antiferromagnetic (AFM) systems, is a phenomenon first discovered in Co/CoO nanoparticles in 1956 [1]. The EB effect has significant impacts on the technological applications of data storage products, spintronic devices, permanent magnets, and many other devices [2–8]. Extensive research has led to the notion that EB must originate from uncompensated interfacial spins that are pinned in the AFM and cannot be reversed by external field after a field-cooling (FC) procedure through the Néel temperature (T_N) of the AFM [9,10]. However, the elusive origin of EB is still not well understood due to the complexity of this effect [9–18].

After the discovery of this effect in Co/CoO nanoparticles, investigations of the EB effects have been mainly focused on a large number of heterogeneous structures such as magnetic bilayers, core-shell nanoparticles, and FM nanoparticles embedded in AFM matrix compounds [6–17]. The EB effects have also been observed in single-phase bulk oxides and alloys with competing exchange interactions which always result in magnetic phase separations or spin-glass states in these systems [18–24]. For example, a zero-field-cooling (ZFC) EB (ZEB) effect has been realized in Ni-Mn-In and Mn-Pt-Ga Heusler alloys [19–21]. The super-spin-glass (SSG) phase and the FM inclusions embedded in the ferrimagnetic (FIM) ordering matrix were proposed to play key roles in Ni-Mn-In [19] and Mn-Pt-Ga [21], respectively. It is obvious that they are all structurally single-phased bulk materials but with multiple magnetic phases, which can give rise to the EB effect by exchange couplings at the interfaces of different magnetic phases. Besides, EB has also been reported in $YbFe_2O_4$ systems with exchange interaction taking place at low temperature between FM Yb^{3+} and FIM Fe^{2+}/Fe^{3+} sublattices [24]. Nevertheless, little research about EB has been done for the bulk metallic materials with exchange interactions occurring among the bulk sublattices [18].

The R-3*d* intermetallics have been proven to be a fertile research area due to their fascinating physical properties, including hard magnetic properties, giant magnetostriction effect, giant magnetocaloric effect, etc. [25–28]. Among them, Mn is the only 3*d* magnetic transition metal that can stabilize binary compounds of $ThMn_{12}$-type structure (space group $I4/mmm$), leading to the highest metal–to–rare-earth ratio in the rare-earth intermetallics [28]. In RMn_{12} compounds, the Mn ions are coupled antiferromagnetically, showing Néel temperatures around 100 K. The substitution of Fe for Mn in $RMn_{12-x}Fe_x$ promotes ferromagnetic ordering [29–32]. The magnetic arrangements of the 3*d* sublattices are antiferromagnetic for $x < 6$; then transform progressively to more complex configurations of "FM + AFM" for $6 < x < 9$; and finally to a purely ferromagnetic one for the iron-rich compounds ($x = 9$) [31]. Therefore, we consider the compound of $RMn_{12-x}Fe_x$ as a single-phase magnet that consists of two kinds of magnetic sublattices: one is AFM structure and another is FM structure, mimicking that of an artificial FM/AFM superlattice. Such a system will be a suitable model for the study of EB with perfect FM/AFM intersublattice exchange coupling which could be easily tuned by the concentration of composed elements.

In this work, we found the existence of an EB effect in rare-earth transition-metal compounds $YMn_{12-x}Fe_x$ ($x = 6.0$–8.8) bulk alloys where the pinning phenomenon is caused by highly homogenous global interaction between FM/AFM sublattices. In $YMn_{4.4}Fe_{7.6}$, with the strongest competing magnetic interactions, the relatively high ordering temperature and low magnetic anisotropy in the AFM lattice lead to a very sharp switching characteristic of the EB effect far below the Néel temperature T_N. Based on the intersublattice interactions, a numerical model was established and was

*Corresponding author: liushunquan@pku.edu.cn

†Corresponding author: jbyang@pku.edu.cn

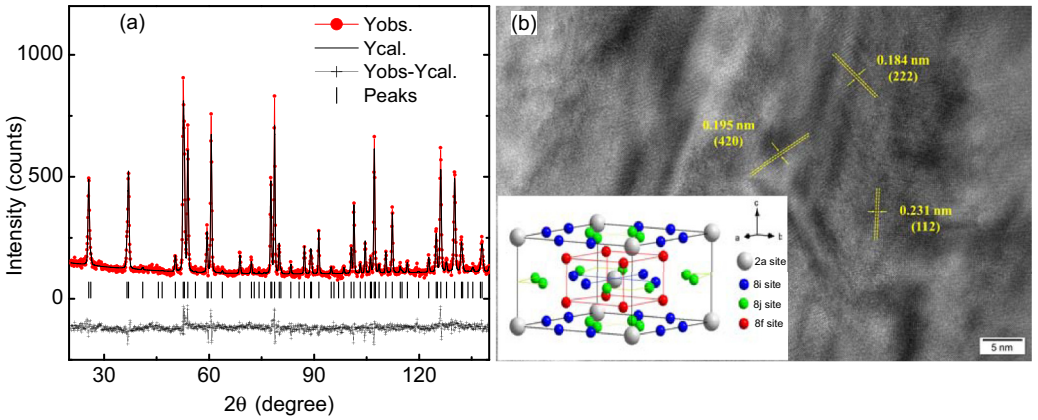

FIG. 1. (a) The high-resolution neutron diffraction pattern of $YMn_{4.4}Fe_{7.6}$ measured at 300 K. Y_{obs} and Y_{cal} represent the observed and calculated curves, respectively. The bottom curve Y_{obs}-Y_{cal} is the difference between experimental data and refinement data. The vertical bars indicate the magnetic (top) and Bragg (bottom) peak positions. The neutron wavelength is 1.884 Å. (b) The HRTEM image of $YMn_{4.4}Fe_{7.6}$ grain. (The insert shows the crystal structure obtained from the refinement of the neutron diffraction data).

found to corroborate well with the experimental results. We demonstrated that the EB effect in this system originates from the intersublattice interactions with high homogeneity.

II. EXPERIMENTAL AND THEORETICAL METHODS

The polycrystalline $YMn_{12-x}Fe_x$ ($x = 6.0$–8.8) bulk samples were prepared by arc melting of 99.9% pure materials in a purified argon atmosphere. An excess rare earth and manganese were added to compensate for their losses during melting. Then the ingots were annealed in an evacuated and sealed silica tube at 1000 °C for 5 days. The crystal and magnetic structures of these compounds were determined using the x-ray diffraction (XRD) with Cu $K\alpha$ radiation and neutron diffraction at various temperatures. High-resolution transmission electron microscopy (HRTEM) images were obtained using a JEOL JEM-2010F microscope at an accelerating voltage of 200 kV. The specimens for TEM were thinned by argon ion milling. Magnetization was measured using a magnetic property measurement system (MPMS-7) and the physical property measurement system (PPMS).

III. RESULTS AND DISCUSSION

The high-resolution neutron diffraction pattern of $YMn_{4.4}Fe_{7.6}$ measured at 300 K is shown in Fig. 1(a). The refinement of XRD and neutron diffraction indicates that the samples ($x = 6.0$–8.6) are a single phase with tetragonal $ThMn_{12}$-type structure (see Fig. 1(b) inset and Fig. S1 [33]), the so-called 1:12 phase, with space group $I4/mmm$ and lattice parameters $a = b = 8.5032(2)$ Å, $c = 4.7645(2)$ Å. The rare earths occupy the $2a$ sites while Fe/Mn atoms occupy three nonequivalent sites: $8i$, $8j$, and $8f$, with strong site preferences that the $8i$ sites favor Mn and the $8f$ sites favor Fe atoms [31,32]. The high-resolution TEM image [Fig. 1(b)] indicates a well-defined lattice structure of a single particle and confirms that the sample is polycrystalline with multiple lattice orientations and interfaces within a single particle.

To characterize the magnetic properties of $YMn_{12-x}Fe_x$ compounds, the temperature dependence of the magnetization (M-T) was measured. Figure 2 shows the magnetic phase diagram of $YMn_{12-x}Fe_x$ ($6.0 \leqslant x \leqslant 8.8$) under a magnetic field of 1.0 kOe according to the M-T data. It can be seen that most of the samples have three transition temperatures corresponding to Curie temperature (T_C, blue triangle), Néel temperature (T_N, red circle), and spin freezing temperature (T_f, black square), respectively. The T_C monotonically increases whereas T_N decreases with the increase of Fe content. Along with the temperature decreasing, the samples experienced paramagnetic, ferromagnetic, antiferromagnetic, and glassy magnetic state changes for $x > 7.6$, and paramagnetic, antiferromagnetic, ferromagnetic, and glassy magnetic state changes for $x < 7.6$. Therefore, the ferromagnetic and antiferromagnetic exchange coupling effect becomes stronger at low temperature. The strongest competition between ferromagnetic and antiferromagnetic interactions can be expected at the crossing point

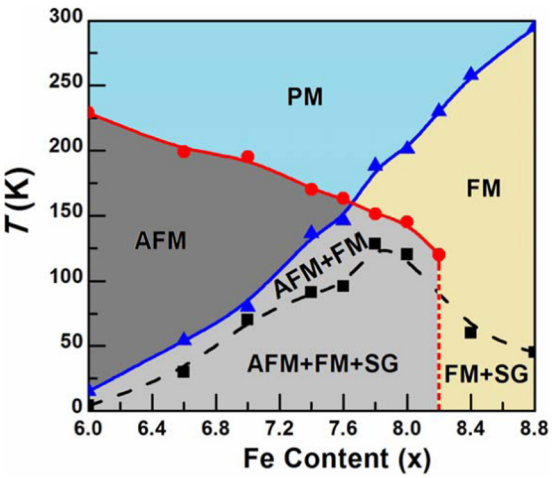

FIG. 2. The magnetic phase diagram of the $YMn_{12-x}Fe_x$($6.0 \leqslant x \leqslant 8.8$) under a magnetic field of 1 kOe. T_C (blue triangle) represents the Curie temperature, T_N (red circle) is the Néel temperature, and T_f (black square) is the temperature corresponding to the bifurcation point in the zero-field-cooling and field-cooling magnetization curves. PM, AFM, FM, and SG represent paramagnetic, antiferromagnetic, ferromagnetic, and spin-glass phases, respectively.

TABLE I. The coercivity H_C and exchange bias field H_E of the $YMn_{12-x}Fe_x$ alloys ($x = 6.0-8.8$) at 5 K with different cooling conditions.

	H_C (Oe)	H_E (Oe)	H_C (Oe)	H_E (Oe)
Cooling field	0 Oe	0 Oe	1 kOe	1 kOe
$YMn_{3.2}Fe_{8.8}$			164	58
$YMn_{3.6}Fe_{8.4}$	132	0	114	663
$YMn_{3.8}Fe_{8.2}$	222	0	60	1483
$YMn_{4.0}Fe_{8.0}$	979	0	409	1934
$YMn_{4.2}Fe_{7.8}$	823	0	284	2489
$YMn_{4.4}Fe_{7.6}$	85	0	81	5956
$YMn_{4.6}Fe_{7.4}$	27	0	23	5180
$YMn_{5.0}Fe_{7.0}$	9889	2802	9821	2876
$YMn_{5.4}Fe_{6.6}$	7429	641	7496	660
$YMn_{6.0}Fe_{6.0}$			472.5	76.5

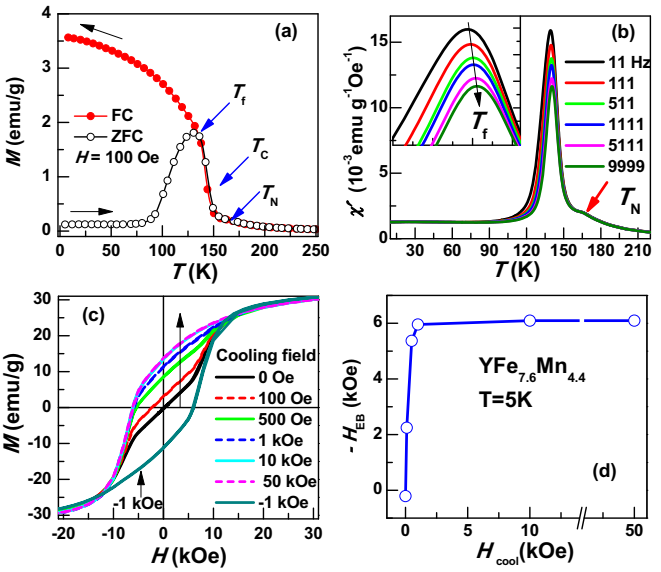

FIG. 3. (a) M-T curves of $YMn_{4.4}Fe_{7.6}$ alloy measured under $H = 100$ Oe after ZFC and FC. (b) The real part χ' of ac susceptibility curve of $YMn_{4.4}Fe_{7.6}$ at different frequencies with ac magnetic field of 10 Oe after ZFC from 300 K. The inset shows the enlarged scale at around 130 K. (c) M-H hysteresis loops at 5 K for $YMn_{4.4}Fe_{7.6}$ under different cooling fields. (d) The dependence of EB on the cooling magnetic field H_{cool} at 5 K.

of the T_C and T_N curves, which corresponds to the highest freezing temperature T_f. This suggests that the competition between ferromagnetic and antiferromagnetic interactions may lead to a large EB effect for the $x \approx 7.6$ sample.

The Fe content dependence of EB effect in the $YMn_{12-x}Fe_x$ alloys ($x = 6.0-8.0$) was investigated. Table I lists the EB fields (H_E) and coercivities (H_C) of the $YMn_{12-x}Fe_x$ alloys ($x = 6.0-8.0$) under FC conditions, where H_E and H_C are defined as $H_E = -(H_L + H_R)/2$ and $H_C = -(H_L\text{-}H_R)/2$, respectively, with H_L and H_R being the left and right coercive fields. It is found that all of the samples show the EB effect under FC conditions. After a 1 kOe FC procedure from room temperature, the H_E value increases with the decrease of Fe content and reaches a maximum of about 5.96 kOe at $x = 7.6$, then decreases with further decrease of Fe content. The maximum H_E corresponds to the strongest competing exchange interaction between the Fe and Mn sublattices. In addition, in the samples with $x = 7.0$ and 6.6, a spontaneous EB effect with large coercivities is found under the ZFC condition and little difference of coercivity H_C and H_E is revealed between FC and ZFC conditions.

Figure 3(a) displays the typical ZFC and FC magnetization curves for $YMn_{4.4}Fe_{7.6}$ under applied field of 100 Oe. The ZFC curve exhibits two peaks at $T_N = 163$ K and $T_f = 130$ K, and there is a bifurcation between the ZFC and FC curves at around T_f. The antiferromagnetic ordering of the Mn ($8i$) magnetic sublattice occurs at $T_N \approx 163$ K. There is another magnetic transition at around 143 K (T_C) due to the ferromagnetic ordering of magnetic moments at Fe ($8f$) and ($8j$) sites. Below 100 K, the ZFC magnetization drops with the decreasing temperature, indicating that the spontaneous interaction between Mn and Fe sublattices prefers an AFM configuration. As shown in Fig. 3(b), from the real part of ac susceptibility curve of $YMn_{4.4}Fe_{7.6}$, two distinct peaks can be observed (the arrows indicate the positions). One peak corresponds to the antiferromagnetic ordering temperature T_N that does not change with frequency; the other peak corresponds to spin freezing temperature T_f that moves with increasing frequency to the high-temperature region. This indicates that the material has the characteristics of a spin glass due to the competing interactions among different magnetic sublattices. What makes the system interesting is that the intersublattice coupling is relatively weak compared to the cooling field and can be manipulated by a FC process under moderate magnetic fields. As shown in Fig. 3(a), after cooling the sample in 100 Oe from 300 K, the FC magnetization goes up instead of dropping down below ~125 K, indicating a parallel alignment of two magnetic sublattices after FC. Thus, the relative orientation between Mn and Fe magnetic sublattices can be effectively manipulated by the FC process. Figure 3(c) shows the M-H hysteresis loops at 5 K for $YMn_{4.4}Fe_{7.6}$ with various cooling fields. The FC M-H loops shift left along H axis with positive fields and shift right along H axis with negative magnetic fields, while the ZFC M-H loop exhibits nearly symmetric coercive fields. The EB field H_E reaches a giant value of 6.1 kOe with a cooling field of 50 kOe for rare-earth-based intermetallics.

We then studied the dependence of EB effect on the cooling field H_{cool} at 5 K. As shown in Fig. 3(d), H_E increases rapidly with the increasing H_{cool} and nearly reaches its saturation value at $H_{cool} = 1$ kOe. With further increase of the cooling field, H_E increases slightly and remains almost constant up to 50 kOe. This feature of cooling field dependence is different from that in the phase-separated oxides or spin-glass systems where H_E decays rapidly with high cooling magnetic fields due to the growth of the FM clusters or the melting of spin glass [18,34,35]. This indicates that in $YMn_{12-x}Fe_x$, the metastable spin configuration is reasonably stable even against the strong external magnetic field. The uniqueness of $YMn_{12-x}Fe_x$ suggests that the observed giant EB may not be an interfacial coupling type resulting from phase separation or spin glass, two major mechanisms for the EB effect in single-phase compounds and alloys that have been reported so far.

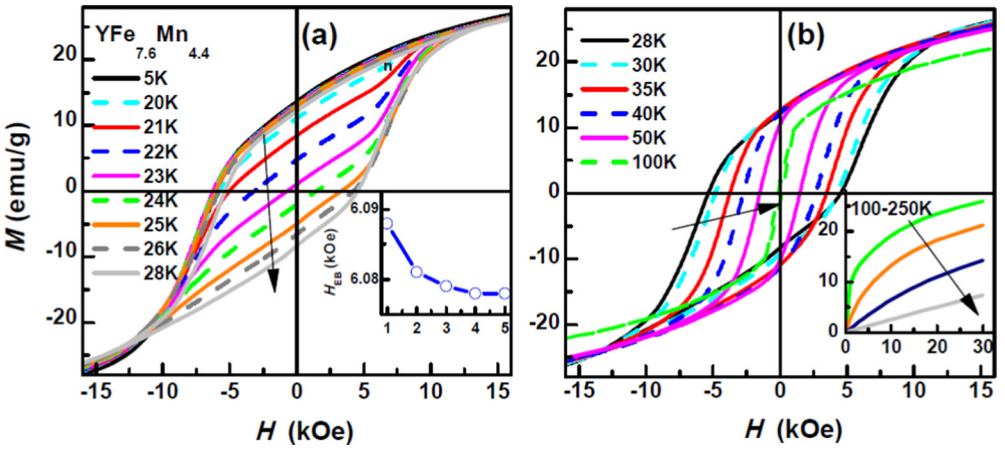

FIG. 4. The hysteresis loops of $YMn_{4.4}Fe_{7.6}$ after field cooling under 10 kOe at temperatures of (a) 5–28 K (the inset shows the training effect of H_E at 5 K) and (b) 28–100 K (the insert shows the M-H curves at 100-250 K).

To further investigate the giant EB effect, we studied the temperature dependence of EB under FC conditions. Figure 4 shows the hysteresis loops of $YMn_{4.4}Fe_{7.6}$ alloy at various temperatures. The characteristics of the hysteresis loops reveal three types of changes with the increasing temperature: (I) in the range of 5–20 K, both branches of the hysteresis loop coincide and show no significant variation with the temperature [in Fig. 4(a)]. (II) In the range of 20–30 K, the left branch of the loop shifts slightly to the left direction, while the right branch shifts quickly along the x axis to the right direction until a symmetric loop forms at about 30 K [in Fig. 4(a)]. (III) Both left and right branches gradually shift back to the original point (0,0) until they coincide with the temperature above 30 K [Fig. 4(b)].

To analyze the impact of temperature on the EB effect, the temperature dependence of H_L, H_R, H_C, and H_E are plotted in Fig. 5. In the temperature range of 5–20 K, both H_L and H_R take the value of about -6.1 kOe and remain almost constant. The value of H_R alters abruptly from negative 5.8 kOe to positive 4.5 kOe in the range of 20–28 K, and then starts to decrease with further increase of the temperature, while the value of H_L decreases gradually after 25 K and reaches zero at about 150 K. In accordance to the changes of H_L and H_R, H_E first maintains at about 6 kOe at $T < 20$ K, then decreases rapidly to -113 Oe at about 32 K, and nearly disappears at the blocking temperature $T_B = 40$ K. The spin freezing temperature T_f [see Fig. 3(a)] of about 120 K is well above T_B, suggesting that the EB effect is not related to the spin-glass phase in this system. The H_C shows a tiny value close to zero at $T < 20$ K, increases abruptly after 20 K, reaches the maximum of 5 kOe at 28 K, and then decreases slowly to close to zero at 150 K. The sharp changes of H_C and H_E at around 25 K are related to the high homogeneity of intersublattice exchange interaction in this system, in which the large EB effect originates from the exchange interaction between different bulk magnetic sublattices.

This interpretation is supported by the negligibly small training effect in $YMn_{4.4}Fe_{7.6}$, where the EB field decreases only 0.16% during the first five consecutive field cyclings at 5 K after FC from 300 K with $H_{cool} = 50$ kOe, just like what the Fig. 4(a) insert shows. In the FM/AFM heterostructures, the

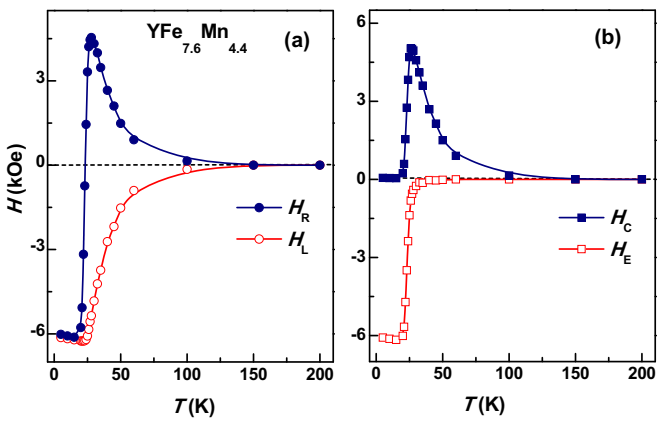

FIG. 5. Temperature dependence of (a) H_L, H_R and (b) H_C, H_E of $YMn_{4.4}Fe_{7.6}$ alloy at 5 K after FC with 10 kOe.

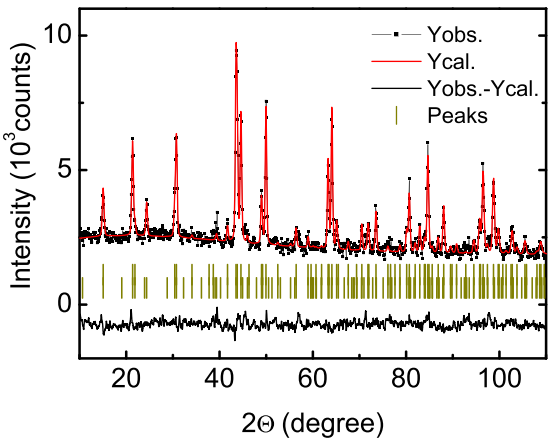

FIG. 6. The neutron diffraction pattern of $YMn_{4.4}Fe_{7.6}$ measured at 10 K. Y_{obs} and Y_{cal} represent the observed and calculated curves, respectively. The bottom curve Y_{obs}-Y_{cal} is the difference between experimental data and refinement data. The vertical bars indicate the magnetic (top) and Bragg (bottom) peak positions. The neutron wavelength is 1.570 Å.

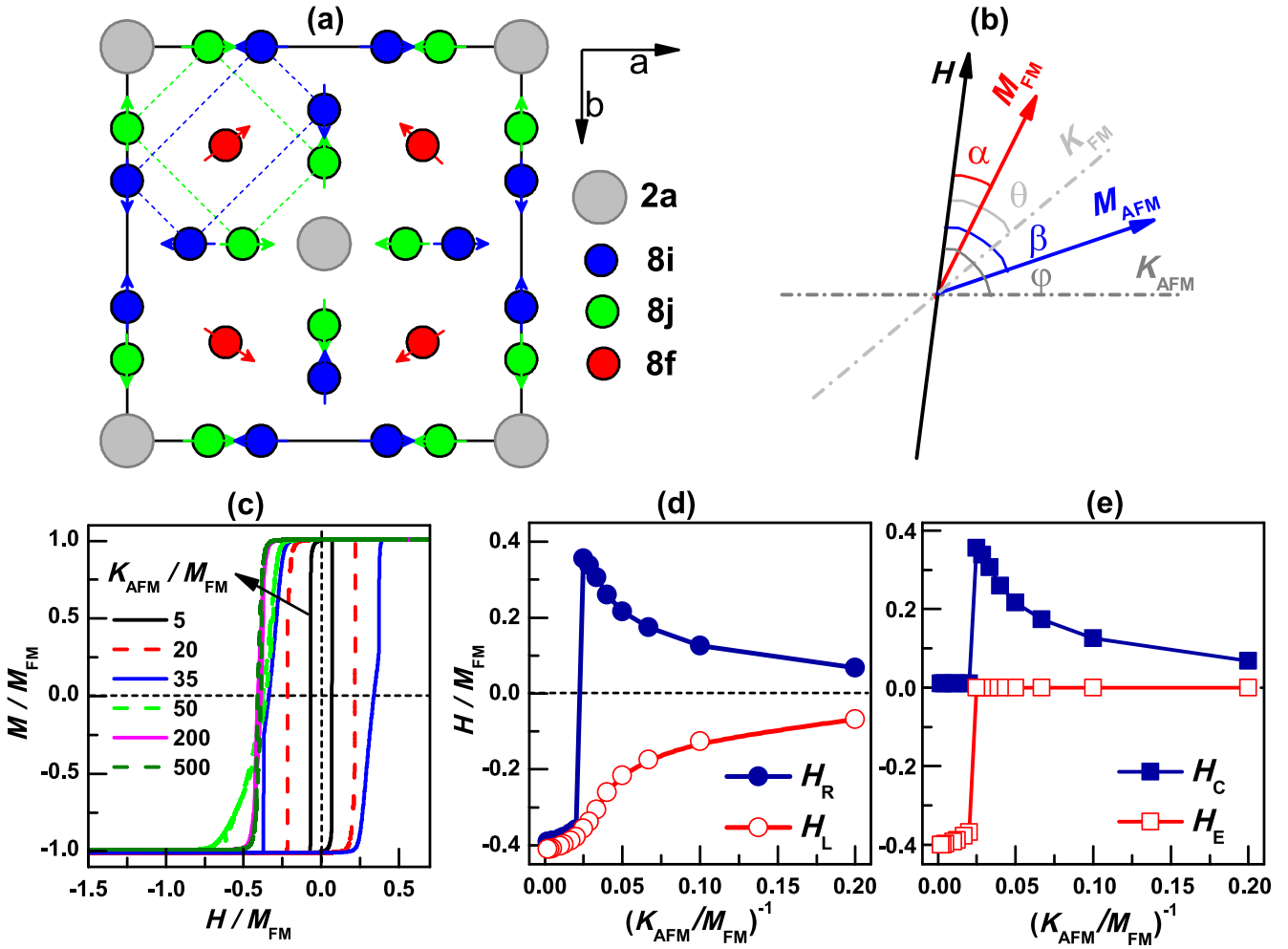

FIG. 7. (a) The schematic magnetic structure of the $YMn_{4.4}Fe_{7.6}$ compound (top view along c axis). (b) Schematic diagram of angles involved in the theoretical model. (c) The calculated magnetic hysteresis loops as a function of K_{AFM}. (d) and (e) The calculated H_L, H_R, H_C, and H_E as functions of K_{AFM}^{-1}.

training effect originates from the heat-activated fluctuations in the FM-AFM exchange coupling, which modify the magnetic interactions between differently coupled regions with each reversal [36–38]. For a system with high homogeneity, all AFM spins act like one macroscopic spin and show no fluctuation. Consequently, there can be only two states in this system: all AFM spins contribute to the EB or no AFM spins contribute to the EB. Thus, the training effect, a state where only a part of the AFM spins contribute to the EB, will be absent in this system. The negligibly small training effect well supports the proposed highly homogenous intersublattice exchange coupling mechanism for the EB in this system, indicating that the bulk AFM lattices play a crucial role in pinning the interfacial uncompensated spins which can give rise to the EB effect.

In order to establish a comprehensive picture of the above results, the $YMn_{12-x}Fe_x$ alloys were considered as a single-phase magnet that consists of two magnetic sublattices, one with AFM structure and another with FM structure. The spin configuration is therefore similar to that of an artificial FM/AFM superlattice. The neutron diffraction pattern of the $YMn_{4.4}Fe_{7.6}$ sample measured at 10 K is shown in Fig. 6. According to neutron diffraction data refinement, the magnetic structure of the $YMn_{4.4}Fe_{7.6}$ is presented in Fig. 7(a), which is consistent with the magnetic structure obtained by Pique *et al.* [31]. The magnetic interactions between Mn-Mn, Fe-Fe, and Mn-Fe are AFM, FM, and AFM, respectively. Fe and Mn atoms prefer to occupy $8f$ and $8i$ sites, respectively, while they randomly distribute on the $8j$ site. Due to the single-phase character of $YMn_{4.4}Fe_{7.6}$, the FM/AFM interface can homogenously distribute between different magnetic sublattices. As can be seen from Fig. 7(a), $YMn_{4.4}Fe_{7.6}$ forms two sets of magnetic lattices: Mn atoms on $8i$ sites give rise to the AFM coupling magnetic sublattice (blue atoms), and Fe atoms on $8f$ sites give rise to the FM coupling magnetic sublattice (red atoms). Mn and Fe atoms on the $8j$ site form the "AFM/FM interface", which leads to AFM interaction between $8j$-$8i$ sublattices, and AFM or FM interaction between $8j$ and $8f$ sublattices with Mn or Fe occupying the $8j$ site, respectively. Due to the fact that the $8j$ site can be occupied by Fe or Mn atoms evenly, the stoichiometry of Fe content directly affects Fe and Mn ratio at the interface and subsequently influences the exchange coupling interaction between AFM and FM sublattices. With the increase of Fe content, the

$8j$ sites (interface) become FM dominated and may lead to smaller H_E and H_C due to a weaker pinning effect of the interface layers. This is confirmed by the results in Table I, where different degrees of EB effect were observed in the samples with different Fe contents.

According to the above discussion, each sublattice of $R\mathrm{Mn}_{12-x}\mathrm{Fe}_x$ can be viewed as a single spin due to its high homogeneity. The generalized Meiklejohn-Bean (M-B) model is adopted to explain the EB in $R\mathrm{Mn}_{12-x}\mathrm{Fe}_x$ compounds, which consists of AFM (Mn atoms from $8i$ site and $8j$ site) and FM (Fe atoms from $8f$ site and $8j$ site) sublattices. The energy of the system is given by [39]

$$\begin{aligned} E = & -J_{\text{FM-AFM}} M_{\text{FM}} M_{\text{AFM}} \cos(\beta - \alpha) \\ & - K_{\text{FM}}[M_{\text{FM}} \cos(\theta - \alpha)]^2 - K_{\text{AFM}}[M_{\text{AFM}} \cos(\varphi - \beta)]^2 \\ & - H M_{\text{FM}} \cos(\alpha) - H M_{\text{AFM}} \cos(\beta), \end{aligned} \tag{1}$$

where H and $M_{\text{FM(AFM)}}$ are externally applied magnetic field and saturation magnetization of FM(AFM) sublattices, respectively. $K_{\text{FM(AFM)}}$ is effective uniaxial magnetic anisotropy constant of FM(AFM) sublattices, $J_{\text{FM-AFM}}$ is the exchange coupling between the FM and AFM sublattices, while α, β, θ, and φ are the azimuth angles of M_{FM}, M_{AFM}, uniaxial anisotropy axis of FM, and uniaxial anisotropy axis of AFM with respect to the applied magnetic field direction, respectively, as Fig. 7(b) shows.

As we know, the temperature dependence of EB is relevant to thermal instabilities of the AFM interfacial magnetization [40]. According to the Néel-Brown relaxation theory, the Néel relaxation time τ_N of the AFM magnetization should be

$$\tau_N = \tau_0 \exp\left(\frac{K_{\text{AFM}} V}{k_B T}\right). \tag{2}$$

Then the contributions to the EB effect from increasing temperature T in our experiment can be analogous to that from the decreasing antiferromagnetic anisotropy K_{AFM} in our calculation model with the relation of $T \approx K_{\text{AFM}}^{-1}$.

According to Eq. (1), the hysteresis loops of $R\mathrm{Mn}_{12-x}\mathrm{Fe}_x (R = Y)$ with different K_{AFM} are calculated and are plotted in Fig. 7(c). The obtained coercivities H_C and the EB fields H_E are shown as the function of K_{AFM}^{-1} in Figs. 7(d) and 7(e). Although a noncollinear magnetic structure was obtained in this system with neutron powder diffraction, the magnetic properties, such as the coercivity, indicate that the magnetocrystalline anisotropy in this system is weak, which can be easily overcome by the external field. After FC, the magnetic moments in ferromagnetic site $8f$ and a part of the magnetic moments in antiferromagnetic site $8i$ and $8j$ will be aligned in the cooling field direction. Thus, a collinear alignment of the anisotropy axes and the external field has been assumed in the calculation, i.e., $\theta = \phi = 0$ in Fig. 7(b). All the parameters are dimensionless with $M_{\text{FM}} = 1$ and $M_{\text{AFM}} = 0.5M_{\text{FM}}$, $K_F = 0.1M_{\text{FM}}, H_{\text{max}} = 2M_F, J_{\text{FM-AFM}} = -4M_{\text{FM}}$. The antiferromagnetic anisotropy K_{AFM} changes between $500M_{\text{FM}}$ and $5M_{\text{FM}}$.

As can be seen from Figs. 7(d) and 7(e), the calculated results, especially the sudden switching-on of the EB field and the sudden switching-off of the coercivity at low temperatures, agree very well with the experimental data (see Fig. 5). When the temperature is lower than 20 K, the anisotropy of the antiferromagnetic spins is so large that the AFM spins remain in their original configuration while the FM spins rotate with the external magnetic field. This will give a loop shift of the ferromagnetic spins due to the unidirectional pining from the antiferromagnetic spins. However, when the temperature is higher than 20 K, the antiferromagnetic spins begin to rotate with the ferromagnetic spins under the interfacial exchange coupling due to the decrease of antiferromagnetic anisotropy K_{AFM} with the increasing temperature. Then the bidirectional pining from the antiferromagnetic spins will give an enhancement in the coercivities of the ferromagnetic spins. The sharpness of the switching process in the experimental results indicates the homogeneity of the FM-AFM interface, corresponding to the special global intersublattice coupling in $\mathrm{YMn}_{4.4}\mathrm{Fe}_{7.6}$.

Our finding provides an abundant system with intersublattice exchange-coupling-induced exchange bias effect. This will justify itself in the application of antiferromagnetic metal spintronics at the level of several lattices [41]. For example, a thin layer of the $\mathrm{R(Mn.Fe)}_{12}$ alloy with homogenous exchange interactions can be used as the conventional spin-valve structure, which may show the advantage of easy manipulation with lower current or external magnetic field. Besides, it also implies the possibility of coercivity enhancement in permanent magnets of high anisotropy near Curie temperatures through exchange coupling with antiferromagnetic counterparts [42].

IV. CONCLUSIONS

To conclude, we have found a tunable giant EB effect in a family of rare-earth–transition-metal intermetallic compounds $\mathrm{YMn}_{12-x}\mathrm{Fe}_x$ ($x = 6.6$–8.8), resulting from a competing magnetic interaction among ferromagnetic (FM) and antiferromagnetic (AFM) sublattices. A maximum EB with a loop shift of up to 6.1 kOe has been revealed in this single-phase bulk alloy $\mathrm{YMn}_{4.4}\mathrm{Fe}_{7.6}$. The EB field remains almost unchanged at temperatures below 20 K but shows a sudden switching-off in the temperature range of 25–30 K, where the coercivity shows a sudden switching-on and a subsequent slow decrease. The calculated results of the numerical model show an excellent agreement with the experimental result of this unique temperature dependence of EB. This indicates that the large exchange anisotropy originates from the highly homogenous exchange interaction between bulk Fe-rich and Mn-rich sublattices. Supporting information is available [33].

ACKNOWLEDGMENTS

This work is supported by the National Key Research and Development Program of China (Grants No. 2016YFB0700901, No. 2017YFA0401502, and No. 2017YFA0206303) and National Natural Science Foundation of China (Grants No. 11504348, No. 51371009, No. 11675006, No. 50971003, and No. 51171001), and the Foundation of Key Laboratory of Neutron Physics of CAEP (Grant No. 2014BB02).

Y.X. and R.W. contributed equally to this work.

[1] W. H. Meiklejohn and C. P. Bean, Phys. Rev. **102**, 1413 (1956).
[2] B. Dieny, J. Magn. Magn. Mater. **136**, 335 (1994).
[3] J. Nogués and I. K. Schuller, J. Magn. Magn. Mater. **192**, 203 (1999).
[4] C. Tsang, T. Lin, S. MacDonald, M. Pinarbasi, N. Robertson, H. Santini, and P. Arnett, IEEE Trans. Magn. **33**, 2866 (1997).
[5] R. H. Koch, G. Grinstein, G. A. Keefe, Y. Lu, P. L. Trouilloud, W. J. Gallagher, and S. S. P. Parkin, Phys. Rev. Lett. **84**, 5419 (2000).
[6] J. Nogués, J. Sort, V. Langlais, V. Skumryev, S. Surinach, J. S. Munoz, and M. D. Baró, Phys. Rep. **422**, 65 (2000).
[7] V. Skumryev, S. Stoyanov, Y. Zhang, G. hadjipanayis, D. Givord, and J. Nogues, Nature (London) **423**, 850 (2003).
[8] J. A. De Toro, J. P. Andrés, J. A. González, P. Muñiz, T. Muñoz, P. S. Normile, and J. M. Riveiro, Phys. Rev. B **73**, 094449 (2006).
[9] S. K. Mishra, F. Radu, H. A. Dürr, and W. Eberhardt, Phys. Rev. Lett. **102**, 177208 (2009).
[10] K. Takano, R. H. Kodama, A. E. Berkowitz, W. Cao, and G. Thomas, Phys. Rev. Lett. **79**, 1130 (1997).
[11] C. L. Chien, V. S. Gornakov, V. I. Nikitenko, A. J. Shapiro, and R. D. Shull, Phys. Rev. B **68**, 014418 (2003).
[12] M. Kiwi, J. Magn. Magn. Mater. **234**, 584 (2001).
[13] R. Morales, Z.-P. Li, J. Olamit, K. Liu, J. M. Alameda, and I. K. Schuller, Phys. Rev. Lett. **102**, 097201 (2009).
[14] P. Miltenyi, M. Gierlings, J. Keller, B. Beschoten, G. Guntherodt, U. Nowak, and K. D. Usadel, Phys. Rev. Lett. **84**, 4224 (2000).
[15] P. Kappenberger, S. Martin, Y. Pellmont, H. J. Hug, J. B. Kortright, O. Hellwig, and E. E. Fullerton, Phys. Rev. Lett. **91**, 267202 (2003).
[16] M. Gibert, P. Zubko, R. Scherwitzl, J. Íñiguez, and J. M. Triscone, Nat. Mater. **11**, 195 (2012).
[17] Z. M. Tian, S. L. Yuan, S. Y. Yin, L. Liu, J. H. He, H. N. Duan, P. Li, and C. H. Wang, Appl. Phys. Lett. **93**, 222505 (2008).
[18] S. Giri, M. Patra, and S. Majumdar, J. Phys.: Condens. Matter **23**, 073201 (2011).
[19] B. M. Wang, Y. Liu, P. Ren, B. Xia, K. B. Ruan, J. B. Yi, J. Ding, X. G. Li, and L. Wang, Phys. Rev. Lett. **106**, 077203 (2011).
[20] T. Maity, S. Goswami, D. Bhattacharya, and S. Roy, Phys. Rev. Lett. **110**, 107201 (2013).
[21] A. K. Nayak, M. Nicklas, S. Chadov, P. Khuntia, C. Shekhar, A. Kalache, M. Baenitz, Y. Skourski, V. K. Guduru, A. Puri, U. Zeitler, J. M. D. Coey, and C. Felser, Nat. Mater. **14**, 679 (2015).
[22] X. D. Tang, W. H. Wang, W. Zhu, E. K. Liu, G. H. Wu, F. B. Meng, H. Y. Liu, and H. Z. Luo, Appl. Phys. Lett. **97**, 242513 (2010).
[23] J. K. Murthy and A. Venimadhav, Appl. Phys. Lett. **103**, 252410 (2013).
[24] Y. Sun, J. Z. Cong, Y. S. Chai, L. Q. Yan, Y. L. Zhao, S. G. Wang, W. Ning, and Y. H. Zhang, Appl. Phys. Lett. **102**, 172406 (2013).
[25] M. Sagawa, S. Fujimura, N. Togawa, H. Yamamoto, and Y. Matsuura, J. Appl. Phys. **55**, 2083 (1984).
[26] V. K. Pecharsky and K. A. Gschneidner, Jr., Phys. Rev. Lett. **78**, 4494 (1997).
[27] A. E. Clark, in *Ferromagnetic Materials*, edited by E. P. Wohlfahrt (North-Holland, Amsterdam, 1980).
[28] J. Deportes, D. Givord, R. Lemaire, and H. Nagai, Physica B+C **86**, 69 (1977).
[29] Y. C. Yang, B. Kebe, W. J. James, J. Deportes, and W. B. Yelon, J. Appl. Phys. **52**, 2077 (1981).
[30] M. Morales, M. Bacmann, P. Wolfers, D. Fruchart, and B. Ouladdiaf, Phys. Rev. B **64**, 144426 (2001).
[31] C. Pique, E. Abad, J. A. Blanco, R. Burriel, and M. T. Fernández-Díaz, Phys. Rev. B **71**, 174422 (2005).
[32] J. B. Yang, W. B. Yelon, W. J. James, Q. Cai, D. Eckert, A. Handstein, K. H. Müller, and Y. C. Yang, Phys. Rev. B **65**, 064444 (2001).
[33] See Supplemental Material at http://link.aps.org/supplemental/10.1103/PhysRevB.96.064440 for the crystal structures and magnetic properties of $RMn_{12-x}Fe_x$ compounds.
[34] D. Niebieskikwiat and M. B. Salamon, Phys. Rev. B **72**, 174422 (2005).
[35] Y. Tang, Y. Sun, and Z. Cheng, J. Appl. Phys. **100**, 023914 (2006).
[36] D. Paccard, C. Schlenker, O. Massenet, R. Montmory, and A. Yelon, Phys. Status Solidi B **16**, 301 (1966).
[37] C. Binek, Phys. Rev. B **70**, 014421 (2004).
[38] T. Gredig, I. N. Krivorotov, and E. D. Dahlberg, Phys. Rev. B **74**, 094431 (2006).
[39] W. H. Meikejoh, J. Appl. Phys. **33**, 1328 (1962).
[40] M. D. Stiles and R. D. McMichael, Phys. Rev. B **60**, 12950 (1999).
[41] E. V. Gomonay and V. M. Loktev, Low Temp. Phys. **40**, 17 (2014).
[42] J. Sort, J. Nogues, S. Surinach, J. S. Munoz, and M. D. Baró, Appl. Phys. Lett. **79**, 1142 (2001).